JOURNAL OF CATALYSIS 154, 137–150 (1995)

Substitution and Stability Effects in Heteropolyacids: A Theoretical Analysis of the Diversity of the Keggin Ion

Shu-Hsien Wang*,[1] Susan A. Jansen,*,[2] and David J. Singh†

*Department of Chemistry, Temple University, Philadelphia, Pennsylvania 19122; and †Department of Chemistry, University of Guyana, Georgetown, Turkeyen, Guyana

Received August 1, 1994; revised December 19, 1994

In this work, the redox effects and stability of a series of analogous $[X^{(n)}Mo_{12}O_{40}]^{(8-n)-}$ and $[X^{(n)}W_{12}O_{40}]^{(8-n)-}$ heteropolyanions are assessed. Both of these homologs display the α-Keggin structure in which a tetrahedral oxyanion helps to satisfy the coordination sphere of the metal oxide octahedron of the clathratic shell. Here, results from a series of semiempirical electronic-structure calculations are used to illustrate the electronic effects induced by chemical modifications. The stability trends produced in this work reliably trace the experimental trends and present the description of electronic features required for stabilization of the Keggin ion. In addition, understanding these electronic effects induced by chemical modification is critical in the rational design of heteropolymetallate catalysts. © 1995 Academic Press, Inc.

INTRODUCTION

Because of their diverse electronic properties, structural chemistries, and multiredox characteristics in oxidation and reduction, the reduced heteropolyanions (HPAs) have received much attention in recent years (1, 2). Most of the heteropolyanions that have been examined were exclusively based on molybdenum or tungsten (2–16) oxide octahedra. They are derived from the oxyacids of the early *d*-block elements displaying high oxidation numbers (3, 4). Two different metallic elements are commonly used in the construction of the well-known cluster cage while multiple heteroatoms sit at the center of the cluster and form the "oxyanion" core. The HPA forms its T_d cage structure through corner- and edge-sharing of MO_6 (M = Mo, W) octahedra, encapsulating one or two heteroatoms as a nucleus (4–7). The typical HPAs, 12 molybdo-heteropolyanions and 12 tungsto-heteropolyanions, displaying T_d symmetry (8) and possessing the general formula $[X^{(n)}M_{12}O_{40}]^{(8-n)-}$ or $[X^{(n)}O_4^{(8-n)-}M_{12}O_{36}]$ (8, 9), are classified as α-Keggin ions where the tetrahedrally coordinated central heteroatom X shares its oxygens with four M_3O_{13} trimers (1, 2, 12). The heteroatom X can be a variety of metallic or intermetallic elements including Al, P, Si, B, and a variety of transition metals (7, 10, 11). The framework of the cluster is formed by condensation of the metal oxide structure, typically MO_3 or M_xO_y or the sodium salt of the oxide (3, 7, 8, 11). As shown in Fig. 1, the structure is composed of two motifs: the trimer and the tetramer. The trimer is formed from three edge-sharing octahedra, and then the trimers share corners to produce the Keggin core. Consequently, there exist four types of oxygens: O_a, O_b, O_p, and O_t (7, 8, 12, 24) as shown in Fig. 1. Two octahedra in a trimer share O_a-bridging atoms and the adjacent trimers bind to each other through O_b-bridging atoms; the O_p apical atoms connect the trimer metal atoms and an X atom, and the O_t terminal atoms display double bond character. Various HPAs are prepared by replacing one or more of the framework metal atoms with the other *d*- or *f*-block elements (4) or by substituting the heteroatom of the central tetrahedron with a representative main group or transition metal element. Normally, this does not compromise the stability or the structure of the HPAs (13) and thus this phenomenon arouses interest in studies of the redox effect and bonding considerations in the electronic structure of the HPAs, and hence, the substitutional influences on the catalytic tendencies of HPAs.

The reduced α-HPAs show a characteristic deep blue color (3, 11, 14) which may result from metal-to-metal and ligand-to-metal charge transfer within the framework of the metal oxide shell. The electrochemical potentials for one- and two-electron reductions are related to the overall charge on the HPAs, and these values suggest that the first two electrons enter the nonbonding metal orbitals of the anion and thus these potentials are nearly independent of the central heteroatom (3, 11, 15) but are dependent on the properties of the shell metals. The reduction process is normally accompanied by protonation and therefore is pH dependent. The addition of hydrogen ion(s) benefits the HPAs by further stabilizing the reduced ion up to a four- or five-electron reduction. Therefore, the magnitude of the charge on the HPAs controls or

[1] Sun Oil Fellow.

[2] To whom correspondence should be addressed.

0021-9517/95 $6.00

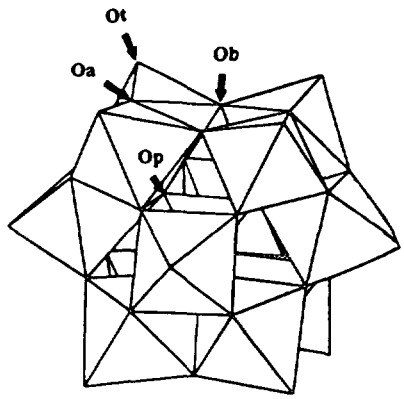

FIG. 1. The α-Keggin ion structure showing four types of oxygens: O_a, edge-shared; O_b, corner-shared; O_p, apical; and O_t, terminal.

modulates the level of reduction that can be sustained by a particular HPA moiety (11, 14).

The substituted heteropolymolybdates and heteropolytungstates are reduced more easily than their all-molybdenum or all-tungsten analogs. Typical metal substitutions include replacement of Mo or W with Ti or V. A correlation between acidity and oxidizing power has been observed for these compounds (15, 16) and it is believed that the bridging oxygens are the active sites (7b, 9) in the oxidative dehydrogenation reaction and in the protonation reaction, and that the oxidation addition reaction involves the terminal oxygen site (7). This is also consistent with results from our previous work on $H_3PMo_{12}O_{40}$ (12).

In this study, we have examined the stabilities and electronic properties of α-Keggin ions as a function of the central heteroatoms and framework metal atoms by treating the structure as a neutral $M_{12}O_{36}$ fragment of the solid oxide with an $X^{(n)}O_4^{(8-n)-}$ trapped at its center (2, 7–16). The results of the extended Hückel molecular orbital (EHMO)/tight binding calculation help to clarify or rationalize the experimental observations and are predictive of the electronic influences of the substitutent framework metal atom(s) and/or the central heteroatom. The redox behavior of the Keggin ion has been considered in this analysis as well. This assessment of electronic character will aid in defining the requisites for catalytic application for these oxide cluster and related oxide materials.

COMPUTATIONAL METHODOLOGY

The computational method used in this study is the crystal band calculation which is an analogue of all-valence molecular orbital procedures based on the semiempirical extended Hückel/tight binding approximation. It was first developed by Hoffmann for the application of organic molecules (17, 18) and then extended by Woflsberg, Helmholz, and others for inorganic species (see Ref. 19). This method has been successful in the analysis of many stable three-dimensional molecular conformations and in studies of local and overall symmetries of molecular orbitals, especially to the extent of delocalization of π orbitals. It has been used to evaluate solid state structures, surface catalytic properties of metals, oxides, and carbide complexes, and interactions or organometallic compounds (20–22). Considering the size and complexity of the Keggin cluster, computational analysis of this problem by extended Hückel formalism provides a reasonable assessment of chemical features. Of course, *ab initio* approaches would provide more quantitative features in the analysis, but on clusters of such size they are of limited application for several reasons. First, the parameterization of the transition metals for a full *ab initio* CI calculation is complicated by the number of potential oxidation states. In addition, the density of molecular states at the frontier in the cluster makes a full or partial CI calculation almost prohibitive at any realistic level. The cluster has over 100 states at or near the frontier. The method selected is well known to provide a good electronic structure analysis. The relative energy effects calculated are predictive of chemical and physical phenomena while the absolute energy terms are less reliable.

The model for the structure is not minimized by extended Hückel protocols; it is extracted from crystallographic data in which atomic positions are identified for every atom of the cluster. In this work, the position of the central heteroatom X was set as an origin of the Cartesian coordinates for convenience and with the actual structural models based on the Keggin cluster geometry extracted from crystallographic data (23). The calculations were performed for the complete cluster, as the size and complexity of the unit cell precludes a complete three-dimensional band analysis. Molecular calculations were performed on the full Keggin ion clusters to produce interaction diagrams. The density of states (DOS) was generated by application of the band component of the EHMACC (extended Hückel molecular and crystal calculation). However, the construct utilized is one in which the translation distance between units exceeds any potential orbital overlap >20 Å. This is a standard computational approach and allows for the generation of the overlap population that occurs and the DOS for the noninteracting clusters. The energies and orbital vectors are identical to those obtained from the molecular calculation. Owing to the cluster size, analysis of the DOS provides a useful and convenient tool, and the interactions are those within the clusters (24).

The extended Hückel input parameters (20–22) used for this work are listed in Tables 1 and 2. The parameters selected were developed by Otamin *et al.* (20), Sandra *et al.* (21), and Vuckovic *et al.* (21) for metal oxides and

TABLE 1

Extended Hückel Parameters Used in the Calculations for Main Group Elements

Element	Orbital	H_{ii} (eV)	Slater exponent
B	2*s*	−15.2	1.3
	2*p*	−8.5	1.3
Al	3*s*	−12.3	1.167
	3*p*	−6.5	1.167
Si	3*s*	−16.3	1.383
	3*p*	−8.5	1.383
Ge	4*s*	−16.0	2.16
	4*p*	−9.0	1.85
P	3*s*	−14.5	1.6
	3*p*	−9.7	1.6
S	3*s*	−18.0	1.817
	3*p*	−11.3	1.817
O	2*s*	−27.61	2.28
	2*p*	−11.01	2.275

metal carbides. These are charge-iterated parameters selected to produce more accurate HOMO (highest occupied molecular orbital) and LUMO (lowest inoccupied molecular orbital) levels in clusters and Fermi levels in solid state. These parameters have been used successfully for vanadium and molybdenum oxides, titanium carbides, and many metal surfaces. In addition, the results obtained here were tested against the "molecular" parameters. The trends produced were identical as the relative effects between the metal orbital energies and oxygen orbital energies are preserved.

RESULTS AND DISCUSSION

In this work, we have carefully considered the effect of chemical composition on the electronic properties of the Keggin ion. In doing so, many structural variants were examined. These include substitution of the primary shell metal and substitution of the central oxyanion. For the former, the molybdenum and tungsten were considered not only because they provide the most stable Keggin ions but because of their unique reactivity (2, 7, 11, 14). For the latter, a variety of main group elements and transition metals have been considered, as it is well known that the "cavity" can accommodate almost any stable tetrahedral oxyanion and that this coordination strongly influences the stability of the cluster and may influence the overall redox stability of the primary shell metal. The parameters by which the electronic effects have been evaluated include a comparison of relative energies for a homologous series, analysis of local bonding effects through consideration of overlap population data, and a consideration of charge localization as a function of redox state. The extended Hückel analysis provides many indicators of stability and bond strength; of course, other methods offer different features for the analysis of bonding parameters. Some methods offer a more precise evaluation of energetic components by considering the electronic exchange and Pauli repulsion; most rely on SCF calculations which are of limited application for very large systems. Since the extended Hückel is a one-electron calculation based on orbital overlap, the parameters obtained in this analysis include the binding energy and the overlap population. The binding energy is computed from consideration of the interaction of the two primary fragments of the Keggin ion, the $M_{12}O_{36}$ shell and the $X^{(n)}O_4^{(8-n)-}$ oxyanion, and is defined as the total energy of the complex less than that of the two isolated fragments. The overlap population is computed by the EHMO/tight binding method; though it is not normalized for any given bond, it serves as a measure of bond strength for a particular bond type (24). The subsequent discussion will be divided into sections in which the heteroatom X is either a main group element/metal or a transition metal.

TABLE 2

Extended Hückel Parameters Used in the Calculations for Transition Metals

Element	Orbital	H_{ii} (eV)	Slater exponent
Mn	4*s*	−9.75	1.8
	4*p*	−5.89	1.8
	3*d*	−9.67	5.15 (0.532)
			1.9 (0.649)
Fe	4*s*	−10.6	1.575
	4*p*	−3.37	0.975
	3*d*	−10.7	5.35 (0.5366)
			1.8 (0.666779)
Co	4*s*	−9.21	2.0
	4*p*	−5.29	2.00
	3*d*	−11.18	5.55 (0.56786)
			2.1 (0.60586)
Cu	4*s*	−9.4	2.2
	4*p*	−4.06	2.2
	3*d*	−12.0	5.75 (0.58)
			2.10 (0.62)
Zn	4*s*	−12.41	2.01
	4*p*	−6.53	1.7
Mo	5*s*	−7.3	1.96
	4*p*	−3.6	1.96
	4*d*	−7.9	4.54 (0.590)
			1.96 (0.590)
W	6*s*	−6.26	2.34
	6*p*	−3.17	2.34
	5*d*	−8.37	4.98 (0.6685)
			2.16 (0.5424)

1. Effects of Main-Group-Substituted Central Ions in the Keggin Unit

Stability of the Unreduced HPAs. In this analysis, the binding energy represents the energy difference realized upon coordination of the $X^{(n)}O_4^{(8-n)-}$ in the $M_{12}O_{36}$ shell and thus should be representative of a significant contribution to the total cluster stability. These changes result from increased bonding interactions between various atoms within the cluster. In other words, this binding energy can be referred to as the "additional" stabilization energy of the Keggin ion when compared to the energy of $M_{12}O_{36}$ shell. These binding energies listed in Tables 3a and 3b range from −4.20 to −6.00 eV for a variety of the main group oxyanions in α-molybdo-Keggin units and are about 0.1 to 0.3 eV lower for the α-tungsto-Keggin ions. These data suggest that the 12 heteropolytungstates are generally more stable than the corresponding 12 heteropolymolybdates (3, 7, 11). The relative stability of heteropolymolybdates is identical to that of heteropolytungstates: $SMo_{12}O_{40}^{2-} > PMo_{12}O_{40}^{3-} > GeMo_{12}O_{40}^{4-} > BMo_{12}O_{40}^{5-} > SiMo_{12}O_{40}^{4-}$. These computed binding energy trends agree with the experimental observations (7, 9, 15).

For an indication of the local bonding effects that provide this increased stabilization, the analysis of overlap population is utilized as it is a relative measure of bond strength. From Tables 4 and 5, it can be seen that the electronic overlap populations between tungsten and oxygen atoms (O_a, O_b, O_p, and O_t) were greater than those between molybdenum and oxygen atoms. This is due to the relative difference in electronegativities of tungsten and molybdenum compared with O, as the W–O bond has a greater degree of covalency than the Mo–O bond (26). In this method, the overlap population and calculated binding energy reach a maximum when orbital overlap is optimal. Therefore, increases in the overlap population and, consequently binding energy can be attributed to a sizable mixture of metal and oxygen states, producing better orbital overlap. These effects are related directly to the relative electronegativities, i.e., orbital energies of the constituent atoms. Furthermore, the electronic character of the central ion affects the bonding between O_p and X and consequently O_p and M. The overall stabilization of the cluster can be characterized by considering these bonding interactions. Interestingly, there is a "trade-off" in bonding between M–O_p and X–O_p, with M–O_p satisfying the octahedral bonding structure of the shell metal M, X–O_p retaining the tetrahedral bonding structure of X, and consequently stabilizing the HPA. A strong correlation between the cluster binding energy and M–O_p bonding is observed. Figure 2 shows a plot of the binding energy versus the M–O overlap population. In this figure, a nearly linear correlation is observed, demonstrating that the primary stabilizing interaction, i.e., M–O_p, does not compromise other bonding features within the cluster to a signifi-

TABLE 3a

Binding Energy and Cluster Assembly Energy (eV) of Main Group Elements

XO_4^{n-}	Binding energy	
	Mo-Keggin	W-Keggin
B(+3)	−5.20	−5.35
Si(+4)	−4.78	−5.01
Ge(+4)	−5.25	−5.41
P(+5), $n = 3$	−5.29	−5.45
P(+5), $n = 2$	−5.27	−5.42
P(+5), $n = 1$	−5.24	−5.40
S(+6)	−5.81	−5.92
Al(+3)	−4.26	−4.55

TABLE 3b

Comparison of Overlap Population, Binding Energy, and Cluster Assembly Energy for Main Group Substituents, X = Al, Si, P, and S, of Keggin Ions

XO_4^{n-}	BE[a]	CAE[b]	M–O_p	X–O_p
		M = W		
Al	−4.55	−307	0.1284	0.5191
Si	−5.01	−305	0.1385	0.6239
P	−5.45	−310	0.1475	0.6450
S	−5.92	−315	0.1532	0.6695
		M = Mo		
Al	−4.26	−280	0.1233	0.5196
Si	−4.78	−279	0.1430	0.6267
P	−5.29	−283	0.1433	0.6481
S	−5.81	−287	0.1501	0.6724

[a] The binding energy in units of eV.
[b] The cluster assembly energy in units of eV.

TABLE 4

Overlap Population between Atoms in Main-Group-Substituted Central Oxyanion of Mo-Keggin

X-in-Ku	Mo–O_b	Mo–O_a	Mo–O_t	Mo–O_p	X–O_p
$Mo_{12}O_{36}$	0.2855	0.3132	0.7074		
$Mo_{12}O_{40}^{8-}$	0.2837	0.3108	0.7005	0.1415	
B(+3)	0.2837	0.3112	0.7005	0.1459	0.5784
Si(+4)	0.2836	0.3102	0.7003	0.1430	0.6267
P, $n = -5$	0.2721	0.3081	0.6978	0.1430	0.4681
P, $n = -4$	0.2779	0.3096	0.6991	0.1431	0.6481
P, $n = -3$	0.2837	0.3112	0.7005	0.1433	0.6481
P, $n = -2$	0.2837	0.3111	0.7005	0.1433	0.6481
P, $n = -1$	0.2836	0.3111	0.7005	0.1433	0.6481
S(+6)	0.2837	0.3111	0.7006	0.1501	0.6724
Ge(+4)	0.2838	0.3113	0.7005	0.1419	0.6571
Al(+3)	0.2840	0.3112	0.7006	0.1233	0.5196

TABLE 5

Overlap Population between Atoms Main-Group-Substituted Central Oxyanion of W-Keggin

X-in-Ku	W–O_b	W–O_a	W–O_t	W–O_p	*X*–O_p
$W_{12}O_{36}$	0.2982	0.3251	0.7513		
$W_{12}O_{40}^{8-}$	0.2970	0.3232	0.7425	0.1450	
B(+3)	0.2970	0.3235	0.7425	0.1499	0.5757
Si(+4)	0.2970	0.3232	0.7423	0.1385	0.6239
P, $n = -5$	0.2815	0.3195	0.7376	0.1468	0.6450
P, $n = -4$	0.2892	0.3215	0.7400	0.1472	0.6450
P, $n = -3$	0.2970	0.3235	0.7424	0.1475	0.6450
P, $n = -2$	0.2969	0.3234	0.7424	0.1475	0.6450
P, $n = -1$	0.2969	0.3233	0.7424	0.1475	0.6449
S(+6)	0.2958	0.3222	0.7397	0.1532	0.6695
Ge(+4)	0.2970	0.3236	0.7424	0.1462	0.6487
Al(+3)	0.2971	0.3230	0.7424	0.1284	0.5191

cant degree. To further understand the stabilization effect of the central ion coordination, we have examined the cluster assembly energies as a function of the main group ion in the tetrahedral central oxyanion. In Table 3b, the *M*–O, *X*–O overlap populations are given with the binding energy of $X^{(n)}O_4^{(8-n)-}$ and the cluster assembly energy. The cluster assembly energy is simply the difference in the total bonding energy of the cluster and that of the individual atomic constituents. A strong correlation is observed between the binding energy and the cluster assembly energy. The experimental stability trends and computed binding and cluster assembly energies agree quite well. Only a small difference in stability occurs when X = Si, which is due to a weak antibonding interaction that develops between Si and W. This effect accounts for the lower cluster stabilization computed for the $SiW_{12}O_{40}^{4-}$. The origin of this interaction will be discussed in detail later.

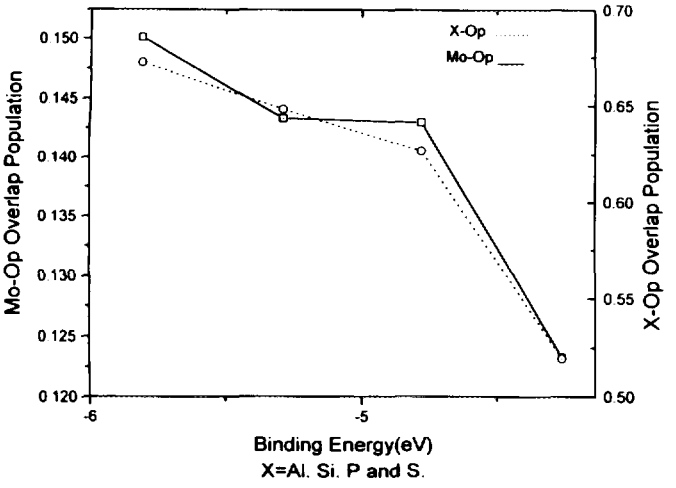

FIG. 2. Correlation diagram of *X*–O_p and binding energy in Mo-based Keggin ions. *X*, central heteroatom.

In the simple octahedral model, one can envisage that the framework metal atoms in Keggin ions use $d_{(x2-y2,z2)}$, s, $p_{(x,y,z)}$ orbitals to form σ bonds with $2p$ orbitals of oxygen atoms. Formally, a double bond exists between *M* and O_t, however, it depends on the local bonding. In a reasonable model, this bond strength can be influenced by the nonbonding oxygen electrons. The same is true for bridging oxygens. Because of this multiple bonding character, there is a dynamic electron transfer or resonance effect between the oxyge $2p$ electrons and the framework metal atoms, enhancing the bonding between *M*–O and thus further stabilizing the *M*–O bond. Many experimental measurements have characterized this "exchange" (2, 7, 11, 26). This may be the main reason that HPAs remain stable under fairly extreme redox conditions and why the oxidation–reduction does not affect local bonding interaction. These nonbonding orbital states sit at ~−11.0 eV, just above the *M*–O bonding states, as seen in the DOS given in Fig. 5, and thus the energy barrier for this type of exchange effect is quite small. For HPA homologs, the electron density on the O_p oxygen reflects the extent of orbital overlap between the framework metal and oxygen atoms and generally indicates the stability of the HPAs (26).

In light of the above discussion, a further consideration of the electron density distribution in the cluster offers some insight into the requisites for catalytic activity. In general, substitution of these central heteroatoms causes little change in the electron density in atoms of the $M_{12}O_{36}$ shell (10, 24). The most pronounced changes occur at the oxygen, O_p, in the central oxyanion. The electron density at the other oxygen sites, O_a, O_b, and O_t, are more critically affected by the choice of the metal atom in the $M_{12}O_{36}$ clathratic shell. This effect arises from the degree of covalent bonding between the metal and oxygen atoms, and seriously influences the stability and lability of the cluster. For instance, the gross populations (Tables 6 and 7) of *X* and O_p in molybdo- and tungsto-polyanions are very close, with the exception of O_p being more reduced in $SiW_{12}O_{40}^{4-}$, i.e., there is 0.4 greater electron charge on the O_p of $SiW_{12}O_{40}^{4-}$ than that of $SiMo_{12}O_{40}^{4-}$. Since there was no significant difference in the overlap population of Si–O and *M*–O_p in both types of HPAs, one might conclude that the reason why $SiW_{12}O_{40}^{4-}$ is more stable than $SiMo_{12}O_{40}^{4-}$ is due to the redox effect or, in other words, the electron transfer between the metal in the clathratic shell and O_p. This increase in electron density at the O_p site is compensated for by decreases in electron density at the oxygen atom sites in the shell. However, owing to the delocalized nature of the oxygen states in the shell, the net loss per oxygen site is quite small and since these states are primarily nonbonding, no change in overlap population is observed.

To "quantify" this effect, changes in the charge distri-

TABLE 6

Gross Population of Main Group Atoms (XO_4^{n-})

	Isolated		Mo-Keggin		W-Keggin	
$X(n)$	X	O_p	X	O_p	X	O_p
B(5)	1.780	7.555	1.965	7.110	1.958	7.081
Si(4)	1.764	7.559	1.923	7.515	1.923	7.116
P(7)	5.053	7.737	2.130	7.071	2.123	7.043
P(6)	4.275	7.681_{avg}	2.130	7.071	2.123	7.043
P(5)	3.497	7.626	2.130	7.070	2.123	7.042
P(4)	2.719	7.570	2.130	7.070	2.123	7.041
P(3)	1.941	7.515	2.130	7.070	2.123	7.040
P(2)	1.939	7.265	2.130	7.070	2.123	7.023
P(1)	1.937	7.016	2.130	7.038	2.123	7.006
S(2)	2.532	7.367	2.733	6.908	2.722	6.881
Ge(4)	1.957	7.511	2.134	7.071	2.128	7.040
Al(5)	1.252	7.687	1.400	7.307	1.410	7.270

bution can be traced from the isolated ion to the complexed ion. Though the magnitude of the charge or electronic population calculated in the extended Hückel scheme is normally exaggerated, the trends in the calculated atomic charge are considered quite valid. For this comparison, the charge on an atom is defined as the difference between its gross population and group number (25). Table 8 shows the gross population of silicon in isolated, molybdo- and tungsto-silicates.

The silicon with +2.236 charge on an isolated central oxyanion was reduced by 0.159 electron charge upon encapsulation in the molybdo- and tungsto-polyanions; O_p with a charge −1.559 of an isolated central oxyanion was only very slightly oxidized to $O_p(-1.515)$ of molybdo- and $O_p(-1.884)$ of tungsto-polyanions. The origin of these phenomena is not obvious. Generally, the M–O_p bond is weak relative to other bonds in the cluster, and for these central oxyanions, the heteroatom X is either nonbonding or slightly antibonding with the framework metal atoms.

TABLE 7

Gross Population of Transition Atoms (XO_4^{n-}) of the First Series

	Isolated		Mo-Keggin		W-Keggin	
$X(n)$	X	O_p	X	O_p	X	O_p
Mn(4)	7.900	6.775	7.799	6.428	7.772	6.395
Mn(1)	6.517	6.371	6.516	6.065	6.513	6.049
Fe(6)	8.150	7.462	6.432	6.920	6.240	6.821
Fe(5)	8.625	7.058	6.427	6.920	6.236	6.821
Co(6)	10.262	7.156	10.315	6.798	10.284	6.754
Co(5)	9.911	6.965	9.960	6.676	9.936	6.636
Cu(7)	11.477	7.631	11.654	7.115	11.615	7.064
Cu(6)	11.778	7.306	11.358	6.961	11.324	6.914
Zn(6)	1.413	7.647	1.564	7.223	1.564	7.191

TABLE 8

Gross Population of Si and O_p Atoms

Element	Isolated oxyanion	$SiMo_{12}O_{40}^{4-}$	$SiW_{12}O_{40}^{4-}$
Si	1.764	1.923	1.923
O_p	7.559	7.515	7.116

In some cases, the X–M interaction becomes appreciable. This effect in polytungstates is greater than that in polymolybdates. The orbital interactions responsible for this effect are shown in Fig. 3. Owing to the increased electronegativity of the tungsten and greater diffuseness of the d-orbitals, this secondary W–X interaction becomes significant. Although the magnitude is not large, it should be noted that 12 such W–X interactions occur. For W, this interaction is antibonding overall; however, the increased net stability in W–O bonding within the cluster offsets the destabilization and hence the cluster demonstrates a higher stability. This effect is the greatest for Si as the orbital states of Si-based oxyanion are energetically more compatible for interaction with those of the metal oxide shell. There are several other subtle differences between $SiM_{12}O_{40}^{4-}$ and $PM_{12}O_{40}^{3-}$. The binding energy (Table 3b) of $SiMo_{12}O_{40}^{4-}$ was −4.78 eV and that of $PMo_{12}O_{40}^{3-}$ was −5.29 eV but, as shown in Table 4, no significant difference in the corresponding overlap populations could be observed within these two heteropolymolybdates except in the local bonding X–O_p of the oxyanion species, i.e., P–O_p >

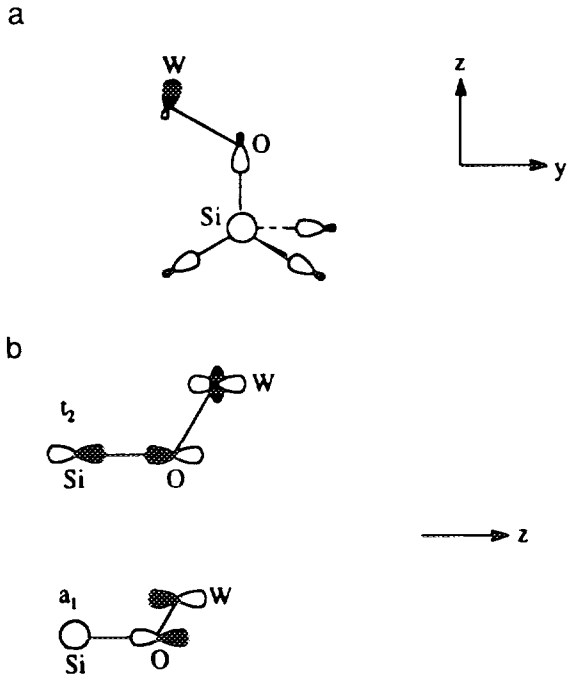

FIG. 3. The orbital representations of the three-way interaction among X (= Si), O_p, and M in $SiW_{12}O_{40}^{4-}$.

Si–O_p, and the antibonding X–Mo, i.e., P–Mo < Si–Mo. Similarly, for heteropolytungstates, the binding energy of silicate was −5.01 eV and that of phosphate was −5.45 eV but, as shown in Table 5,the only differences in bonding occurred with the oxyanion as described above. It appears the silicate is stabilized in the $M_{12}O_{36}$ shell by a mechanism that "strengthens" Si–O bonding in the central tetrahedral oxyanion while the difference in M–Si relative to M–P bonding is probably due to electronegativity effects; Si is less electronegative than P and thus the contribution of Si to the bonding a_1 and t_2 states of the $X^{(n)}O_4^{(8-n)-}$ is less. Upon complexation, a "rehybridization" of the orbitals occurs, changing the relative contribution of Si. There is a "three-way" interaction (24) of the a_1 and t_2 orbitals occurring at the bottom level of the metal–oxygen bonding orbitals among Si, O_p, and M (M = Mo, W) of $SiM_{12}O_{40}^{4-}$ due to the "short" distance (~3.2 Å) between Si and M. This distance is within the limits of the sums of the van der Waals radii and therefore moderate interactions between Si and M develop. Figure 3 clearly shows that the a_1 orbital is composed of Si (s), O_p (p_z), and M (d_{z^2}) orbitals and the t_2 orbitals are composed of Si (p_z), Op (p_z), and M (d_{z^2}) orbitals. In both a_1 and t_2 orbitals, i.e., t_2 of $SiMo_{12}O_{40}^{4-}$ and $SiW_{12}O_{40}^{4-}$, the Si–O_p and W–O_p bonds are net bonding in nature; however, the overall interaction of Si and the framework metal is antibonding. In the a_1 orbital, the magnitude or contribution of W (d_{z^2}) is greater than that of Mo (d_{z^2}) and thus the antibonding character of Si–W is greater than that of Si–Mo. Consequently, the Si–W is more antibonding when compared to the corresponding Si–Mo interaction. Evidence for such effects is also seen in the DOS (Fig. 4): When compared to $SiMo_{12}O_{40}^{4-}$, the tungsten and oxygen bands are more diffuse and dispersed to a lower energy. The W–Si antibonding states develop through the three-way interaction discussed previously and have similar energy. These states become populated, leading to a slightly lower electron density in nonbonding oxygen states, since even the "most extreme" antibonding interactions of the W–Si bond cannot compromise the W–O_p bonding. This effect should be similar for substituents of comparable electronegativities, though W–Si interaction is antibonding. $SiW_{12}O_{40}^{4-}$ is more stabilized than $SiMo_{12}O_{40}^{4-}$ by 0.24 eV due to the greater covalency in W–O bonds.

Reduction of HPAs. Thus far, the bonding effects for a series of common Keggin ions have been discussed. It is important to understand how the cluster is affected upon reduction and how the level of reduction influences the catalytic activity. We have demonstrated that trends in stabilization energy can be directly attributed to somewhat localized M–O_p bonding and that the extent of this bonding depends on the relative electronegativity of the heteroatom X in the tetrahedral oxyanion. To understand

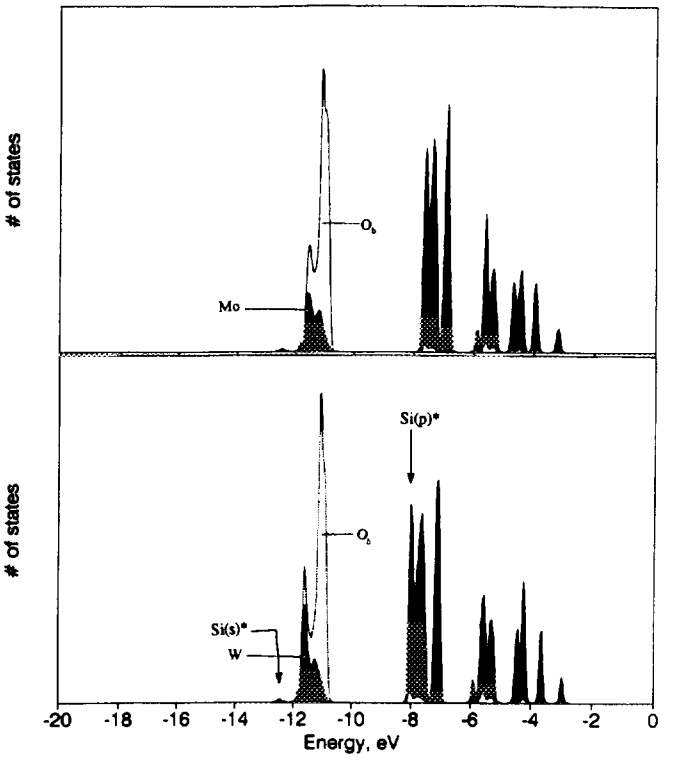

FIG. 4. The projected DOS of $SiM_{12}O_{40}^{4-}$ (M = Mo, W). Here, the contribution of Si is less than 1% of total DOS.

the electron localization/delocalization effects we have considered a model in which a highly charged tetrahedral oxyanion has been placed at the center of the clathratic $M_{12}O_{36}$ shell. The redistribution of electron density and the effect on local bonding interactions can be followed by the indicators described above. This model will prove useful in the consideration of transition metal substitution where multiple-redox states are commonly observed as well. A cursory analysis of the electron density distribution of the Keggin ion as a function of the main metal group in the oxyanion shows that the only significant difference in charge distribution occurs at the O_p site, localized in the tetrahedral ion.

For an initial comparison and as a reference, the overlap population of X–O_p in an isolated oxyanion and in Keggin ions shows that the highly reduced isolated phosphate ions are grossly destabilized; however, a similar reduction on molybdo- and tungsto-phosphates showed only a slight destabilizing effect, as the additional electrons were distributed to the M–O shell, probably to the nonbonding oxygen and metal states of the clathratic shell. This is formally equivalent to a three-electron reduction of the Keggin ion, as observed electrochemically. Here, the highly reduced oxyanion is not meant to be a chemically realistic species but is provided as a reference point to evaluate redistribution of charge.

To assess the effect of redox state on the clathratic nature of the $M_{12}O_{36}$ shell, we have considered insertion of reduced forms of PO_4^{n-} into $M_{12}O_{36}$. Although the isolated reduced forms of PO_4^{n-} where $n > 3$ are less stable than the PO_4^{3-}, the "extra" electrons will relocalize into the clathratic shell upon complexation. The calculated binding energies (Table 3b) show that the increased stability is observed for the reduced PO_4^{n-} as the electrons from antibonding "electronic" PO_4^{n-} states are transfered to nonbonding states of the framework metal in $M_{12}O_{36}$. This observation can be represented by two simple equilibria expressions, using the phosphate Keggin ion as an example:

$$[M_{12}O_{36}]^0[PO_4]^{7-} \rightleftharpoons [M_{12}O_{36}]^{4-}[PO_4]^{3-} \quad [1]$$

$$[M_{12}O_{36}]^0[PO_4]^{3-} \rightleftharpoons [M_{12}O_{36}]^{3-}[PO_4]^0. \quad [2]$$

Clearly, the limits in electronic population lie between these extremes.

The redox effect can be traced further by following the gross populations or charges through the complexation process. The gross population (Table 6) of the reduced, isolated PO_4^{7-} showed that there was a slightly negative charge on phosphorus and thus weakened O_p–P bonding. This can be seen in the overlap population data for the P–O_p bond (Table 4). For PO_4^{6-} and PO_4^{5-}, this effect was not great; however, the redox effect did not attenuate the antibonding interactions enough to stabilize the P–O_p bonds. As for the oxidized PO_4^{2-} and PO_4^{-}, both were stabilized by effective orbital overlap between phosphorus and oxygens.

The order of the total electronic energy of molybdo- and tungsto-polyanions was identical, that is, $PM_{12}O_{40}^{5-} < PM_{12}O_{40}^{4-} < PM_{12}O_{40}^{3-} < PM_{12}O_{40}^{2-}$. This corresponded to the stabilization energy which increases with an additional negative charge on the cluster. In other words, the binding energy of phosphoropolyanions decreased against the pseudo-oxidation state on the phosphorus of the polyanions. The one-electron reduction product was more stable than the reference, $PM_{12}O_{40}^{3-}$; the one- and two-electron oxidation products were as stable as the reference. There was no significant difference in overlap population between M–O_t and P–O_p of $PM_{12}O_{40}^{n-}$ (n = 1 to 7), indicating that the redox effect occurred in the Keggin "shell," not at the central heteroatom. This was observed in comparisons of the overlap population of isolated and Keggin ions also. The Keggin unit can be significantly reduced, perhaps by at least six electrons, without decomposition. Further redox reactions implicate states of the central heteroatom or framework states of the metal oxide shell and thus the stability of the cluster is compromised. In fact, the cluster energies, both the binding and assembly energies, are almost independent of charge on the PO_4^{n-} ion for phosphoro-polyanions. For $PMo_{12}O_{40}^{n-}$ with n = 1 to 5, the gross population of phosphorus was identical. This is also true for oxygen atoms except O_p of $PM_{12}O_{40}^{-}$. Similar effects were seen for tungstophosphoro-polyanions, with the difference in O_p population ranging from 0.018 to 0.035. For an overall charge $n < 3$, the nonbonding oxygen states are depopulated but for $n > 3$, the nonbonding framework metal states become populated. This is further evidence in support of the stability of the multiredox states of the Keggin ions and helps to explain their diverse electrochemistry (7, 11, 14). One- and two-electron reduction products are observed for $PMo_{12}O_{40}^{3-}$ and $PW_{12}O_{40}^{3-}$ with the former occurring more readily. In fact, for both molybdo- and tungsto-Keggin ions, the third electron reduction can be carried out in an acidic solution where reduction is accompanied by protonation and the overall ionic charge on the molecule is kept low (3a).

Significant changes in the electron population of P are also observed. As mentioned before, in the isolated PO_4^{n-} (n = 2 to 5), the gross population (Table 6) of P and O_p was different from that of the polyanions. The difference in electronic population of P decreased from 1.367 for $PO_4^{5-}/PM_{12}O_{40}^{5-}$ to 0.191 for $PO_4^{2-}/PM_{12}O_{40}^{2-}$ and the difference in that of O_p decreased from 0.556 for $PO_4^{5-}/PM_{12}O_{40}^{5-}$ to 0.211 for $PO_4^{2-}/PM_{12}O_{40}^{2-}$.

Implications for catalysis. Such effects have serious implications in catalysis. In the solid state structure, the Keggin ions are assembled in a porous matrix, in which the hydration lattice provides a cohesive framework. If they are on a support, the solid state framework is destroyed and the catalytic site becomes the surface of the Keggin ion (7b). The heteropolyacids are strong acids (7b, 27). On the Hammett scale, their acidity is roughly −8 (7b), while that of sulfuric acid is −12 (28) and that of a typical catalytic zeolite is ~−4. This acidity stems from both Lewis acid sites which are coupled to metal counters and the Brønsted acid character common to protonic acids. The Brønsted acid character can be modified by ion exchange of the protonic species in the acid with simple alkali or transition metal ions or more complex organic cations. The Lewis acid character is more critical as mechanistic steps in the catalytic process require electron transfer and strong interaction with the surface. The tungsto-HPAs tend to have much higher Lewis acidities than those of the molybdo-HPAs, while the molybdic acids possess a slightly higher Brønsted acidity. These differences are likely due to the electron density distribution and acceptor states in the metal oxide. Molybdenum is more highly charged in the HPA, thus contributing to greater Brønsted acidity; however, the difference in the metal charges between tungsten and molybdenum does not account for the observed differences in acidity. The Lewis acidity is influenced by many factors in the cluster.

One important factor is the energy of the acceptor states. Recall that the states initially affected upon reduction are nonbonding metal states. These states are at a considerably lower energy in the tungstates, ~0.8 eV, relative to those in the molybdate clusters. The work of Dronskowski (29), and Dronskowski and Hoffmann (30) provides a way to extract acidity and bond reactivity by considering frontier orbital effects and decomposing these effects into components. Applying this model to these materials does not prove as interesting as in others because the frontier character is almost identical within the molybdate or tungstate series. The hardness indices are 1.42 and 1.61 for tungsten- and molybdenum-based clusters, respectively. This difference is observed as the LUMO levels of the tungstate cluster fall almost 1 eV lower than those of the molybdates. No significant differences are observed in the O *p*-states near the HOMO level between the molybdates and tungstate clusters. In addition, only slight perturbations are identified with central atom substitution. The bond reactivities are assessed for the different types of oxygen; this is effectively done by considering how bond strength changes upon oxidation or reduction. This approach is parallel to that of Dronskowski and Hoffmann. Since oxidation or reduction affects frontier orbital population, the comparison of overlap population as a function of cluster redox offers a nearly equivalent analysis of bond reactivity and profiles the relative orbital contribution to the frontier (12).

Furthermore, the differences in covalency in the two clusters affect the electron distribution at the metal and oxygen sites. In the catalytic nomenclature, the oxygen sites are divided into so-called "electrophilic" and "nucleophilic" sites. These assignments were made based on observed reactivities and indicate relative electron density or charge localization effects. The electrophilic oxygens tend to have a lower negative charge than the nucleophilic oxygens. It is known that the relatively "more electrophilic" bridging oxygens are catalytically active and serve as the oxidative sites of the redox reaction; the hydrogenation and reduction reactions appear to occur at the terminal oxygens which are more nucleophilic. The electrophilicity increases when tungsten is substituted as the framework metal as the overall electron density falls at the oxygen sites. When the hydrogenation or reduction occurs, the framework metal ion pushes the electron density at the M = O site toward O and forms the M–OH bond, which changes the lattice structure and also changes the electronic properties of the active sites. When oxidation occurs, one of the M–O bonds of the M–O–M linkage is broken, releasing the O of the M–O–M bond, and the electron-deficient M will be reduced and subsequently be reoxidized. The M–O bond is reformed by the oxidant, usually O_2, added in the reactant stream. The tungsto-type Keggin ions are more stable than the molybdo-type Keggin ions and, therefore, require application of higher pressure and temperature to activate the oxidation process. They are more commonly used as acid catalysts at lower temperatures or in homogeneous reactions (2b, 7b). The level of reduction of the Keggin ions can compromise the catalytic activity in two ways: The first, and perhaps the most obvious, consequence of reduction is the loss of stability of the ion. It is well documented that at high levels of reduction (12) i.e., more than three electrons, the stability of the Keggin shell for $PMo_{12}O_{40}^{3-}$ and $SiMo_{12}O_{40}^{4-}$ is reduced, with the M–O_a bonds being most critically affected. Reduction limits the Lewis acidity by populating the acceptor states of the metal but can also activate the M–O bond for oxidation processes. Thus, a balance between M–O bonding and redox state must be maintained for optimization of catalytic activity.

In addition to the applications on solid support, many Keggin clusters have been utilized in crystalline form. The crystalline form for most acids and salts of the Keggin ion are constructed by the interconnection of the oxide clusters by water molecules. In these materials, the level of hydration in the crystal appears dependent on the charge on the cluster; the more negative charge on the Keggin unit, the more water molecules in the lattice structure are necessary to stabilize the Keggin unit (7b). Thus the crystal stability is dependent on charge and redox state as well.

It should be noted that parallels in reactivity have been noted for several related metal oxides. For example, prereduction of V_2O_5 is proposed to promote certain oxidation reactions (20). This prereduction assists in the chemisorptive processes and contributes to necessary bond activation. Metal dopants in MoO_3 have been used to augment catalytic activity. In these applications, an electropositive metal is doped into the system to partially reduce the metal state. This component of our analysis suggests that bonding within the metal-oxide shell may be more critical in defining the catalytic activity of the Keggin ion and substitution of the central ion with a main group element does not produce observable effects in electron distribution or bonding. The critical factor affected by this substitution is the overall cluster stability which must be considered when considering the reaction conditions.

2. *Effects of Transition-Metal-Substituted Central Ions in the Keggin Unit*

The previous discussion suggests that modulation of catalytic properties can be achieved by redox control and substitution. A natural progression in the design and control of the catalytic properties of the Keggin ions is to develop new systems based on transition metal oxyanions. Several species have been produced synthetically.

TABLE 9

Binding Energy (eV) of First Transition Metal Elements

XO_4^{n-}	Mo-Keggin	W-Keggin
Mn(+4)	−8.0954	−8.2950
Mn(+7)	−3.7296	−3.8292
Fe(+2)	−7.4980	−8.0611
Fe(+3)	−5.9159	−6.6459
Co(+2)	−4.6949	−4.9370
Co(+3)	−4.5427	−4.7523
Cu(+1)	−1.9776	−2.2610
Cu(+2)	−2.2480	−2.5040
Zn(+2)	−4.7239	−4.9033

TABLE 11

Overlap Population between Atoms in Transition-Metal-Substituted Central Oxyanion of Mo-Keggin

X-in-Ku	Mo–O_b	Mo–O_a	Mo–O_t	Mo–O_p	X–O_p
$Mo_{12}O_{36}$	0.2855	0.3132	0.7074		
$Mo_{12}O_{40}^{8-}$	0.2837	0.3108	0.7005	0.1415	
Mn(+4)	0.2839	0.3118	0.7007	0.1214	0.8051
Mn(+7)	0.2841	0.3121	0.7017	0.1074	1.0231
Fe(+2)	0.2754	0.3136	0.6958	0.1328	0.5105
Fe(+3)	0.2809	0.3150	0.6976	0.1328	0.5108
Co(+2)	0.2835	0.3114	0.6997	0.1565	0.5282
Co(+3)	0.2839	0.3119	0.7005	0.1317	0.5956
Cu(+1)	0.2835	0.3114	0.6993	0.1592	0.3830
Cu(+2)	0.2835	0.3114	0.6997	0.1565	0.4361
Zn(+2)	0.2839	0.3117	0.7006	0.1372	0.5541

Thus far, systems have been prepared in which MnO_4^{-} and CuO_4^{6-} have occupied the central ion site. Clearly, these objectives may produce materials with a greater range of activity and stability and thus consideration of both realized and potential materials is appropriate in light of the preceding discussion. Here, we have considered the effects of substitution of a variety of transition metals on cluster stability, analyzed the new orbital states introduced by the tetrahedral metal oxide, and considered the effect of the redox state of the metal on the electronic properties of the cluster.

As in the case of the reduced phospho-polymetallates, $P^{(n)}MO_{40}^{(8-n)-}$, one of the most significant effects observed was that the overall redox state of the central transition metal or transition metal oxyanion critically affects the stability of the cluster. The calculated stability order of heteropolymolybdates with transition metal oxyanions follows a periodic trend (Table 9). In general, earlier transition metal tetrahedra produced more stable Keggin ions though variation in the redox states of the metal affects the stability. Again, the heteropolytungstates of α-Keggin structure are more stable than the corresponding heteropolymolybdates.

For the first transition series, the stability of the central heteroatom was analyzed for the common oxidation state(s) of the metal. This effect was traced through analysis of the overlap population of the M–O_p in the Keggin unit, except for the Cu^{2+}/Cu^{+} pair (Tables 10, 11, and 12). The stability appears to be dominated by the tetrahedral crystal field stabilization energy (CFSE). For instance, in the cluster with MnO_4^{7-} as the central ion, the overlap population between M–O_p was the smallest and that of X–O_p was the largest among the examined molybdo- and tungsto-polyanions,which indicated that the weakest bonding occurred between the tetrahedral structure and the Keggin ion, while retaining the strongest bonding in the tetrahedron. As a result, the isolated tetrahedral structure scarcely contributed to the stability of the complete

TABLE 10

Average Charges on Keggin Shell Metals (Mo, W)

	Gross population$_{avg}$		Charge$_{avg}$	
XO_4^{n-}	Mo	W	Mo	W
Mn(+4)	1.818	2.169	4.182	3.831
Mn(+7)	1.782	2.020	4.218	3.980
Fe(+2)	1.973	2.237	4.027	3.763
Fe(+3)	1.897	2.165	4.103	3.835
Co(+2)	1.819	2.079	4.181	3.921
Co(+3)	1.812	2.011	4.188	3.989
Cu(+1)	1.825	2.078	4.175	3.922
Cu(+2)	1.822	2.076	4.178	3.924
Zn(+2)	1.794	2.035	4.206	3.965

TABLE 12

Overlap Population between Atoms in Transition-Metal-Substituted Central Oxyanion of W-Keggin

X-in-Ku	W–O_b	W–O_a	W–O_t	W–O_p	X–O_p
$W_{12}O_{36}$	0.2982	0.3251	0.7513		
$W_{12}O_{40}^{8-}$	0.2970	0.3232	0.7425	0.1450	
Mn(+4)	0.2970	0.3237	0.7421	0.1255	0.8109
Mn(+7)	0.2973	0.3242	0.7441	0.1095	1.0207
Fe(+2)	0.2835	0.3218	0.7306	0.1326	0.5840
Fe(+3)	0.2908	0.3237	0.7337	0.1327	0.5840
Co(+2)	0.2969	0.3240	0.7412	0.1452	0.5332
Co(+3)	0.2970	0.3240	0.7417	0.1361	0.5980
Cu(+1)	0.2966	0.3236	0.7401	0.1656	0.3905
Cu(+2)	0.2967	0.3237	0.7408	0.1624	0.4419
Zn(+2)	0.2971	0.3238	0.7424	0.1417	0.5522

Keggin unit and further destabilized the Keggin unit by populating M–O_p bonding states, that is, by inducing further reduction. For MnO_4^{4-}, the overlap population of M–O_p was greater than, and the overlap population of X–O_p fell relative to, that of MnO_4^{7-}. This suggests that the optimum occurs upon satisfying bonding of both M–O_p and X–O_p and thus leading the HPA to the most stable conformation. In general, the overlap population of M–O_p was the driving force of the stability of the Keggin ion but this does not explain why MnO_4^{4-} showed the greatest stability among the first transition series; neither did the tetrahedral CFSE effect. At this redox level, all antibonding states of the Keggin unit remain unoccupied. Therefore, to preserve the Keggin unit, the bonding in the tetrahedron has to be maintained and this depends on the total redox state of the Keggin unit. In addition, the M–O_p bonding has to be developed to an appreciable level. This latter consideration depends on the relative electronegativity of the central atom regardless of whether the central heteroatom is a transition metal or a main group element.

Since the total energy and orbital overlap can be affected by the choice of VSIP (valence state ionization potential) for the substituent metals, which are part of the parameterization (Table 2) of the central heterometal (CHM) the stability trends were tested by using two sets of parameters. Although the energy for an HPA with metal parameters of its CHM was less stable than that with organometallic parameters, the destabilization effect was less than 0.5%; the binding energies calculated from both parameters were very close and the stability trends were virtually identical with the previous conclusions. No significant changes were observed in O_p gross populations and overlap populations upon the variation in the parameters. The rather slight differences in the observed effects for the various parameters were due to the fact that the nonmetallic parameters may treat the metals as a bit too "electronegative" relative to O and P parameters. Therefore, for instance, the Mn^{4+} with metal carbide parameters was reduced more than Mn^{4+} with metallic parameters, though this only slightly affected O_p.

The orbital interaction diagrams show the relationships among X, $X^{(n)}O_4^{(8-n)-}$, and $X^{(n)}M_{12}O_{40}^{(8-n)-}$. First, the valence orbitals of X are stabilized by forming chemical bonds with four oxygen ligands and were further stabilized by interacting with the Keggin shell. For instance, Fig. 5 shows that the s character of aluminum dominates the a_1 and t_2 orbitals in both isolated and Keggin ions but the p character appears to contribute much less. As for the nonmetal central heteroatom, the contribution of the s character to the a_1 orbital was similar to that of the p character to the t_2 orbitals in both isolated and Keggin ions. Here, we use $SiM_{12}O_{40}^{4-}$ as an example (Fig. 6). For the transition metals, however, the relative metal contribution was greater, i.e., the d character was greater in e, t_2, and even a_1 orbitals. Copper showed a significant s contribution to the a_1 orbital while the e and t_2 orbitals possessed a significant admixture of d character (Fig. 5). This will help to explain the small stabilization energy of $Cu^{(n)}M_{12}O_{40}^{(8-n)-}$, as shown in Fig. 7.

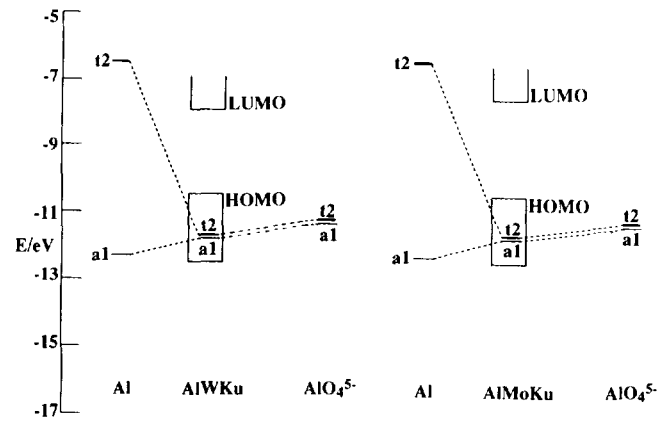

FIG. 5. Correlation diagram of Al, AlO_4^{5-}, and $AlM_{12}O_{40}^{5-}$ (M = Mo, W).

Second, the orbital energies of a_1, e, and t_2 for the tetrahedral oxyanions in the polymolybdates were very close to those of polytungstates, with the energies of the highest occupied molecular orbitals (HOMOs) and the lowest unoccupied molecular orbitals (LUMOs) almost identical, as the character of the fronter orbitals is controlled by the framework metal of a Keggin ion. There was no HOMO–LUMO gap in various substituted Keggin ions, as the e or t_2 states of the metal "intrude" between the M–O bonding and antibonding states of the metal oxide shell. As Eqs. [1] and [2], suggest, electron transfer may occur between the $M_{12}O_{36}$ shell and the central oxya-

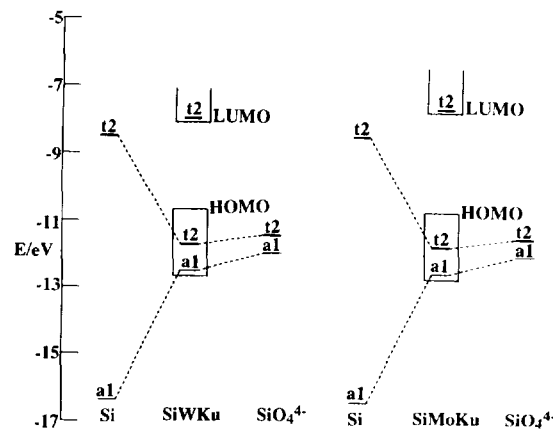

FIG. 6. Correlation diagram of Si, SiO_4^{4-}, and $SiM_{12}O_{40}^{4-}$ (M = Mo, W).

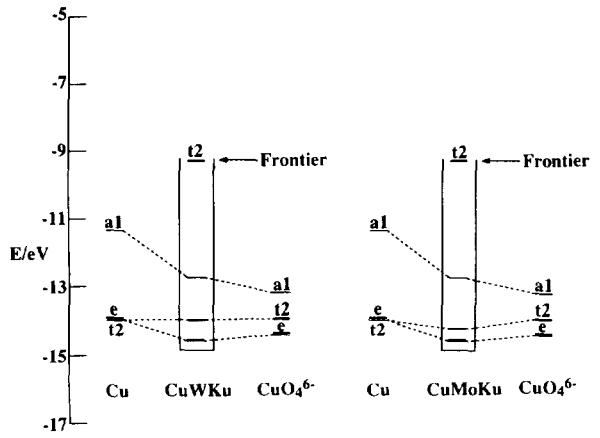

FIG. 7. Correlation diagram of Cu, CuO_4^{6-}, and $CuM_{12}O_{40}^{6-}$ (M = Mo, W).

nion. This was not an active process for the non-metal-based ions. However, for the transition-metal-based anions, the frontier levels of the tetrahedron are very close in energy to the HOMO level of the $M_{12}O_{36}$ shell. Thus, electron redistribution between the $M_{12}O_{36}$ and the $X^{(n)}O_4^{(8-n)-}$ occurs readily. For molecular species, it is generally accepted that the greater the HOMO–LUMO gap, the more stable the species. The collapse of the HOMO–LUMO gap for these materials might be disastrous except for the fact that the "intruder" states are nonbonding states of the tetrahedral central oxyanion. Defect states between the HOMO and LUMO of the Keggin shell occur for Cu. This can be identified easily in Fig. 8, which shows the DOS of $Cu^{(n)}M^{12}O_{40}^{(8-n)-}$. These states are a_1 orbitals. Interestingly, the populations of these states are affected by reduction before those of the cluster. The potentials of one-electron oxidation–reduction would be similar if Keggin ions possessed similar frontier orbitals. For the transition metal oxyanions, states of the tetrahedral ion fall between the oxide and metal bands, thus creating a series of "defect" states that should be redox active and that may further stabilize the structure. This is particularly true for the late transition metals in which the effect is offset by higher d-orbital populations.

A study of the DOS for an aluminate and cuprate will further evidence the important differences in electronic character. Not surprisingly, the DOSs of polymolybdates and polytungstates were similar. In short, the bonding oxygen p-states of the Keggin ion were spread to a greater extent for all four types of oxygen atoms and the DOS was split and broadened at −11.01 eV by d-states of the framework metals. The p band of O_t contributed more states and that of O_p contributed the least number of states among four types of oxygens. This observation indicated that O_t, of more negative charge, was a nucleophilic oxygen which coordinated to an octahedrally bonded framework metal with a short double bond and the O_p had the longest bond with the framework metal.

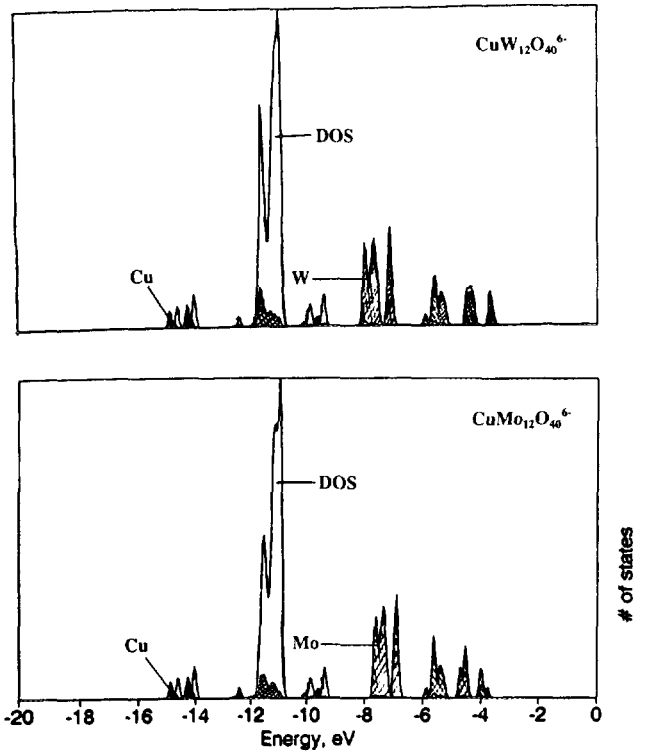

FIG. 8. Density of states for $CuM_{12}O_{40}^{6-}$ (M = Mo, W).

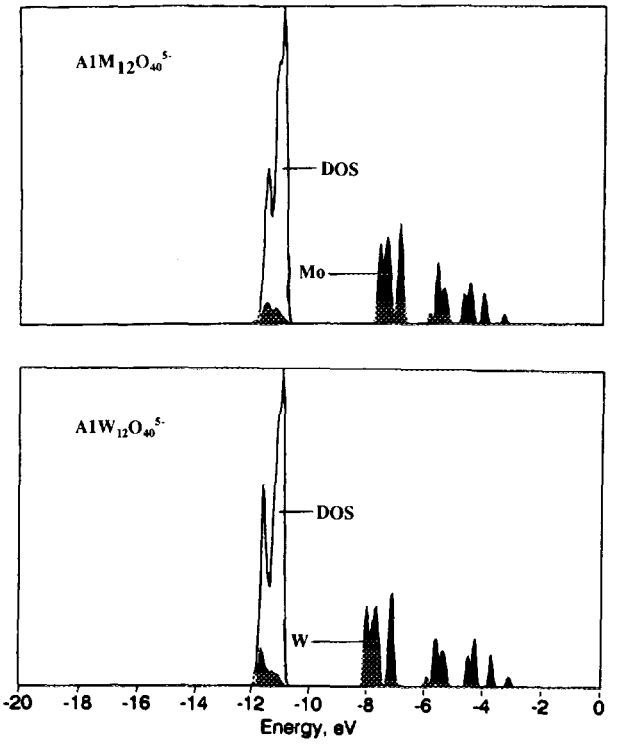

FIG. 9. Density of states for $AlM_{12}O_{40}^{6-}$ (M = Mo, W).

The nonbonding and antibonding bands of a Keggin ion were composed of *s* and *p* bands of the framework metals. Figure 9 shows that the oxygen *p* band of $AlM_{12}O_{40}^{5-}$ was not dispersed by the heteroatom; for the nonmetal central heteroatom, the oxygen *p* band of $X^{(n)}M_{12}O_{40}^{(8-n)-}$ was significantly dispersed by the more electronegative transition metal. The lower levels of this *p* band were more stabilized by stronger covalent bonds while the upper energy levels were more destabilized. The dispersion in the oxygen *p* band is simply due to increased orbital interaction within the tetrahedral center, which reaches a maximum for Fe.

Sizable effects are observed in the charge at the metal center with substitution of the central oxyanion. In general, the charge on Mo or W increases, i.e., becomes more positive, with the electronegativity of the metal of the central oxyanion. This can be seen readily in Table 10. Though these differences span only about 5% per metal site, the overall effect may be significant as there are 12 metals in the framework shell. Since the primary effect is still localized to the states of the tetraderon and the electron transfer effects occur between the nonbonding states of shell and the central oxyanion core, the metal–oxygen bonding in the framework is not affected by this substitution.

There are serious implications for catalysis, however. The more stabilized the tetrahedron, the less stable the Keggin ion becomes, through sacrifice of the O_p–*M* bond. Generally speaking, the catalyst is more active if it possesses a critical stabilization energy for practical usage, and it is necessary to consider the usable lifetime of the catalyst. Changes in electron density at the framework metal will affect both the Brønsted and Lewis acidities of the catalyst, as described previously. The Lewis acidity may be affected more critically, however, as the new acceptor levels, being localized at the central oxyanion core and appearing at the orbital frontier, compete with the acceptor levels of the framework metal atoms. At the same time these materials may be more redox stable and thus will be of greater use in oxidation reactions. The solid state structures may be of further interest as the crystal lattice is affected by the extent of hydration, which depends on the charge of the Keggin ion and the charge localization in the shell.

CONCLUSION

In this work, stability and bonding effects have been described for a series of clusters with the α-Keggin structure. The role of each constituent metal was described with respect to bonding and stability. Though the tungstates were more stable in the native oxidation state, they are more susceptible to reduction than the molybdenum analogs. The analysis of stability with respect to the central oxyanion established that the stability of the cluster is related to the stability of the central oxyanion and the development of reasonable bonding between the tetrahedral central oxyanion and the shell of the cluster, suggesting that the loss of this interaction will lead to degradation of the Keggin unit. The computed stabilization energies traced experimental stability trends well. The analysis of redox effects and electron density distribution allowed a discussion of requisites of activity for both active sites for both oxidation and acid catalysis, and suggested that the selection of a transition metal for the central oxyanion core must be made with caution to preserve the activity of the species.

ACKNOWLEDGMENTS

The authors gratefully acknowledge the help from Messrs. Russ DiFlavia and Mark Kemmerer to maintain the network of VAX/VMS, and the assistance from Mr. Mark Malaty in the preparation of the manuscript.

REFERENCES

1. (a) Katsoulis, D. E., Tausch, V. S., Pope, M. T., *Inorg. Chem.* **26,** 215 (1987); (b) Khan, M. I., Chen, Q., Zubieta, J., *Inorg. Chem.* **32,** 2924 (1993).
2. (a) Fournier, M., Thouvenot, R., Rocchiccioli-Deltcheff, C., *J. Chem. Soc. Faraday Trans.* **87,** 349 (1991); (b) Pope, M. T., Müller, A., *Angew. Chem. Int. Ed. Engl.* **30,** 34 (1991).
3. Kepert, D. L. "Comprehensive Inorganic Chemistry" (J. C. Bailar, Ed.), Chap. 51. Pergamon, New York, 1973.
4. Shriver, D. F., Atkins, P. W., Langford, C. H., "Inorganic Chemistry." Freeman, New York, 1990.
5. Rocchiccioli-Deltcheff, C., Fournier, M., Franck, R., Thouvenot, R., *Inorg. Chem.* **22,** 207 (1983).
6. Thouvenot, R., Fournier, M., Franck, R., Rocchiccioli-Deltcheff, C., *Inorg. Chem.* **23,** 598 (1984).
7. (a) Moffat, J. B. *Polyhedron* **5,** 261 (1986); (b) Misono, M., *Catal. Rev.-Sci. Eng.* **29,** 269 (1987).
8. (a) Matsumoto, K. Y., Kobayashi, A., Saaaki, Y., *Bull. Chem. Soc. Jpn.* **48,** 3146 (1975); (b) Cotton, F. A., Wilkinson, G., "Advanced Inorganic Chemistry: A Comprehensive Text." Wiley, New York, 1980.
9. Evans, H. T., Jr., "Perspectives in Structural Chemistry" (J. D. Dunitt and J. A. Ibers, Eds.), New York, 1971.
10. Sanchez, C., Livage, J., Launay, J. P., Fournier, M., Jeannin, Y., *J. Am. Chem. Soc.* **104,** 3194 (1982).
11. Pope, M. T., "Heteropoly and Isopoly Oxometallates." Springer-Verlag, Berlin, 1983.
12. Jansen, S. A., Singh, D. J., Wang, S.-H., *Chem. Mater.* **6,** 146 (1994).
13. Chauveau, F., Doppelt, P., Lefebvre, J., *Polyhedron* **1,** 263 (1982).
14. (a) Wang, E. B., Zhang, L. C., Wang, Z. P., Huang, R. D., Zhang, S. X., Lin, Y. H., *Gaodeng Xuexiao Huaxue Xuebao.* **13,** 1017 (1992); (b) Pope, M. T., Varge,G. M., Jr., *Inorg. Chem.* **5,** 1249 (1996); (c) *Inorg. Synth.* **27,** (1990).
15. Hodnett, B. K., Moffat, J. B., *J. Catal.* **91,** 93 (1985).
16. Lapham, D., Moffat, J. B., *Langmuir* **7,** 2273 (1991).
17. Hoffamnn, R., *J. Chem. Phys.* **39,** 1397 (1963).
18. Jolley, W. L., "Modern Inorganic Chemistry." McGraw-Hill, New York, (1991).
19. Wagniere, G. H., "Introduction to Elementary Molecular Orbital

Theory and to Semiempirical Methods (Lecture Notes in Chemistry)." Springer-Verlag, New York, (1976).
20. Otamiri, J., Andersson, A., Jansen, S. A., *Langmuir* **6,** 365 (1990).
21. Sanda, P. N., Dove, D. B., Ong, H. L., Jansen, S. A., Hoffmann, R., *Phys. Rev. A* **39,** 2653 (1989).
22. Vuckovic, D. Lj., Jansen, S. A., Hoffmann, R., *Langmuir* **6,** 732 (1990).
23. Yamase, T., Ozeki, T., Motomura, S., *Bull. Chem. Soc. Jpn.* **65,** 1453 (1992).
24. Wang, S.-H., Jansen, S. A., *Chem. Mater.* **6,** 2130 (1994).
25. Mulliken, R. S., *J. Chem. Phys.* **23,** 1833 (1955).
26. Wang, Z. W., Wu, N. J., *Huaxue Xuebao* **49,** 788 (1991).
27. (a) Saito, Y., Cook, P. N., Niiyama, H., Echigoya, E., *J. Catal.* **95,** 49 (1985); (b) Ghosh, A. K., Moffat, J. B., *J. Catal.* **101,** 238 (1986); (c) Umansky, B., Engelhardt, J., Hall, W. K., *J. Catal.* **127,** 128 (1991); (d) Arata, K., *Adv. Catal.* **37,** 165 (1990); (e) Izumi, "Zeolite, Clay and Heteropoly Acid in Organic Reactions." VCH, Weinheim, Germany, 1993.
28. Douglas, B., McDaniel, D., Alexander, J., "Concepts and Models of Inorganic Chemistry," p. 232 Wiley, New York, 1994.
29. Dronskowski, R., *J. Am. Chem. Soc.* **114,** 7230 (1992).
30. Dronskowski, R., Hoffmann, R., *Inorg. Chem.* **31,** 3107 (1992).